Comparison of techniques for computing shell-model effective operators

Michael Thoresen, Petr Navrátil,* and Bruce R. Barrett
Department of Physics, University of Arizona, Tucson, Arizona 85721
(Received 1 October 1997)

Different techniques for calculating effective operators within the framework of the shell model using the same effective interaction and the same excitation spaces are presented. Starting with the large-basis no-core approach, we compare the time-honored perturbation-expansion approach and a model-space truncation approach. Results for the electric quadrupole and magnetic dipole operators are presented for ^{6}Li. The convergence trends and dependence of the effective operators on differing excitation spaces and Pauli Q-operators are studied. In addition, the dependence of the electric-quadrupole effective charge on the harmonic-oscillator frequency and the mass number, for $A=5,6$, is investigated in the model-space truncation approach.
[S0556-2813(98)07606-7]

PACS number(s): 21.60.Cs, 21.30.Fe, 27.20.+n

I. INTRODUCTION

While considerable effort has been devoted to derive the effective interaction used in the shell-model calculations from the nucleon-nucleon interaction [1–3], less work has been done to understand the effective operators employed in calculating different nuclear, usually electromagnetic, properties. A microscopic derivation of effective operators has been only partially successful. It is well known that effective proton and neutron charges must be employed to describe the E2 transitions and moments. These charges are quite different from the free nucleon charges; typically the values of $e^{\rm p}_{\rm eff}\approx 1.5e$ and $e^{\rm n}_{\rm eff}\approx 0.5e$ are obtained for both light and heavy nuclei. It should be noted that these effective charges correspond to a severe truncation to a single-major-shell, or $0\hbar\Omega$, space. Attempts to derive these charges microscopically, usually by perturbation theory [3], or by an ''expanded shell-model'' approach [4], yielded much smaller values. We note that in the ''expanded shell-model'' approach, typically results of a $(0+2)\hbar\Omega$ calculation were truncated to the $0\hbar\Omega$ space to derive the effective charges.

In a previous paper we described a truncation procedure for determining effective charges in small shell-model spaces using the results of large-space no-core calculations [5]. In that study, we used a $6\hbar\Omega$ model space for ^{6}Li, i.e., including excited states up to $6\hbar\Omega$ above the unperturbed ground-state configuration. This procedure yielded $0\hbar\Omega$ effective charges consistent with empirical values. Since previous microscopic perturbation-theory calculations have typically produced effective charges, which are too small compared with the empirical values, it is of interest to compare perturbation-theory calculations and calculations in a truncated model-space in an attempt to understand the reason for these differences.

To carry out this study we propose to perform three calculations: (1) no-core, (2) perturbation theory, and (3) model-space truncation, all using the same nucleon-nucleon potential and assumptions for determining the nuclear reaction matrix G. In addition, to shed more light on the harmonic-oscillator-frequency and the mass-number dependence, we supplement the ^{6}Li results of Ref. [5] with calculations for other $\hbar\Omega$ values and also present new results for $A=5$ system.

In Sec. II we describe the formalism used in performing the three calculations. The no-core results are presented in Sec. III. The perturbation calculation results and the model-space truncation results are discussed in Secs. IV and V, respectively. Conclusions are given in Sec. VI.

II. FORMALISM

All three approaches used in the study begin with the calculation of the Bruckner reaction matrix (or G-matrix) defined as

$$G(\varepsilon)=V+V\frac{Q^P}{\varepsilon-H_0}G(\varepsilon). \tag{1}$$

Either the starting energy ε is parametrized by

$$\varepsilon=\epsilon_a+\epsilon_b+\Delta, \tag{2}$$

with Δ being independent of ϵ_a and ϵ_b, or the dependence of the G-matrix on ε is removed by taking into account the folded diagrams by means of the Lee-Suzuki [6] approach following the procedure described in Ref. [7]. In Eq. (1), V is the free nucleon-nucleon (N-N) interaction. The starting energy ε represents the initial energy of the two nucleons in the medium. H_0 is the unperturbed Hamiltonian of the system, and Q^P is the Pauli projection operator, which projects onto two-particle states that are not already occupied. The G-matrix is evaluated using the method of Barrett, Hewitt, and McCarthy [8], which is similar to the reference-spectrum method [9], in that a reference matrix G^R is calculated and the reaction matrix, or G-matrix, is then obtained by matrix inversion. The computation of the G-matrix employed in our calculations uses the Nijmegen II or the Reid93 N-N interaction [10] in a two-particle Q^P-space shown in Fig. 1 and defined such that

*On leave of absence from the Institute of Nuclear Physics, Academy of Sciences of the Czech Republic, 250 68 Řež near Prague, Czech Republic.

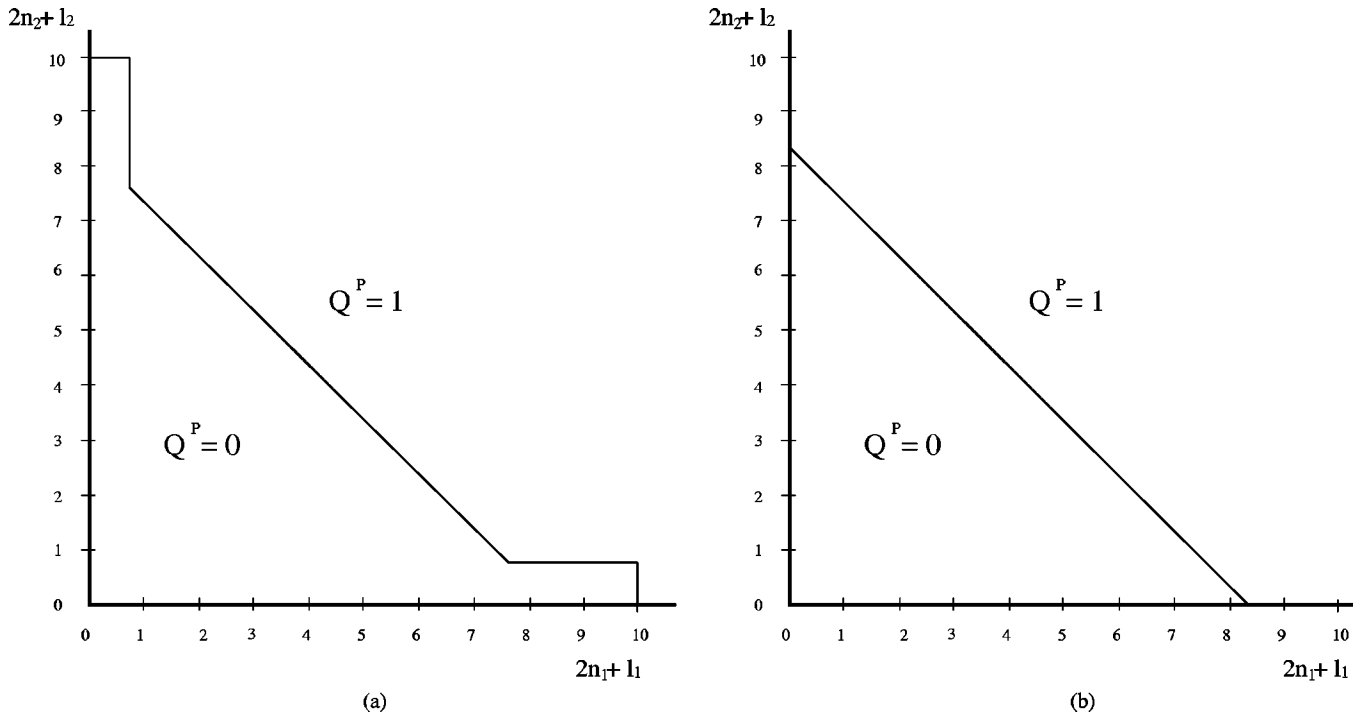

FIG. 1. Q^P-space projection operator for a $6\hbar\Omega$ calculation of ^{6}Li (a) with wings and (b) without wings.

$$Q^P=0 \quad \text{for} \quad (N_1+N_2)\leqslant N_{\max}, \quad N_1=0, \quad \text{or} \quad N_2=0, \quad (3)$$

$$Q^P=1 \quad \text{for all other} \quad N_1 \quad \text{and} \quad N_2,$$

with

$$N_1=2n_1+l_1 \quad \text{and} \quad N_2=2n_2+l_2.$$

In most calculations we use $N_{\max}=8$. Setting $Q^P=0$ for $N_1+N_2\leqslant 8$ forces the intermediate excitations to have an energy greater than $8\hbar\Omega$. We will refer to the G-matrix calculated with a Q^P-space defined this way as an $8\hbar\Omega$ G-matrix. Setting $Q^P=0$ for $N_1=0$ or $N_2=0$ prevents us from scattering into intermediate states that are in the $0s_{1/2}$ state, which is already fully occupied. Hence, the Pauli exclusion principle prevents us from scattering into these states. These portions of the Q^P-space are referred to as the ''wings'' of the Q^P-projection operator. In calculations which do not assume there is a fully occupied ^{4}He core, these $0s_{1/2}$ states may be accessible and the wings may not be needed in the calculation of the G-matrix. For calculations without wings we use the Q^P-operator of Fig. 1(b) defined such that

$$Q^P=0 \quad \text{for} \quad (N_1+N_2)\leqslant N_{\max}. \quad (4)$$

In theory the wings should extend to infinity, but computational limits necessitate putting a finite limit on the extent of the wings. Barrett, Hewitt, and McCarthy [8] investigated truncating the wings at different values and found that there is little effect in extending the wings past $N=10$. Consequently, in our study we have truncated the wings at $N=10$. Because we obtain slightly different G-matrix elements, when we use different Q^P-operators, we will study the effect that including wings has on the calculations. For the purpose of comparison, both the no-core and the perturbation-expansion calculations are done with and without wings.

A. No-core approach

The no-core approach refers to large-basis shell-model calculations performed in a model space of several major harmonic-oscillator shells. In this approach all A nucleons of a given nucleus are active for a complete $N\hbar\Omega$ basis space with a large value for N [11]. (An $N\hbar\Omega$ basis space is one which includes all allowed configurations up to an energy of $N\hbar\Omega$ above the unperturbed ground state.) Due to the no-core assumption, the effective interaction used in the calculations is simplified as no hole states are present. In the approach taken, the effective, in general A-body, interaction is determined for a system of two nucleons only and subsequently used in many-nucleon calculations. As discussed in the beginning of this section, either the two-nucleon G-matrix with a particular parametrization of the starting energy or the two-nucleon G-matrix with the folded diagrams taken into account by means of the Lee-Suzuki approach is employed as the two-body effective interaction in our no-core shell-model calculations. By working in a complete $N\hbar\Omega$ basis space with a single-particle harmonic-oscillator Hamiltonian as our unperturbed Hamiltonian, we can guarantee that all excluded configurations involve an energy of at least $(N+2)\hbar\Omega$, which should limit any intruder-states difficulties to the less interesting physical states higher in the spectrum [12]. That is, the larger the value of N, the better the guarantee that we have included the major configurations making up the physical low-lying states. Using complete $N\hbar\Omega$ harmonic-oscillator spaces allows us to project out the spurious center-of-mass components in the wave functions [13–15]. Note, however, that the calculations using

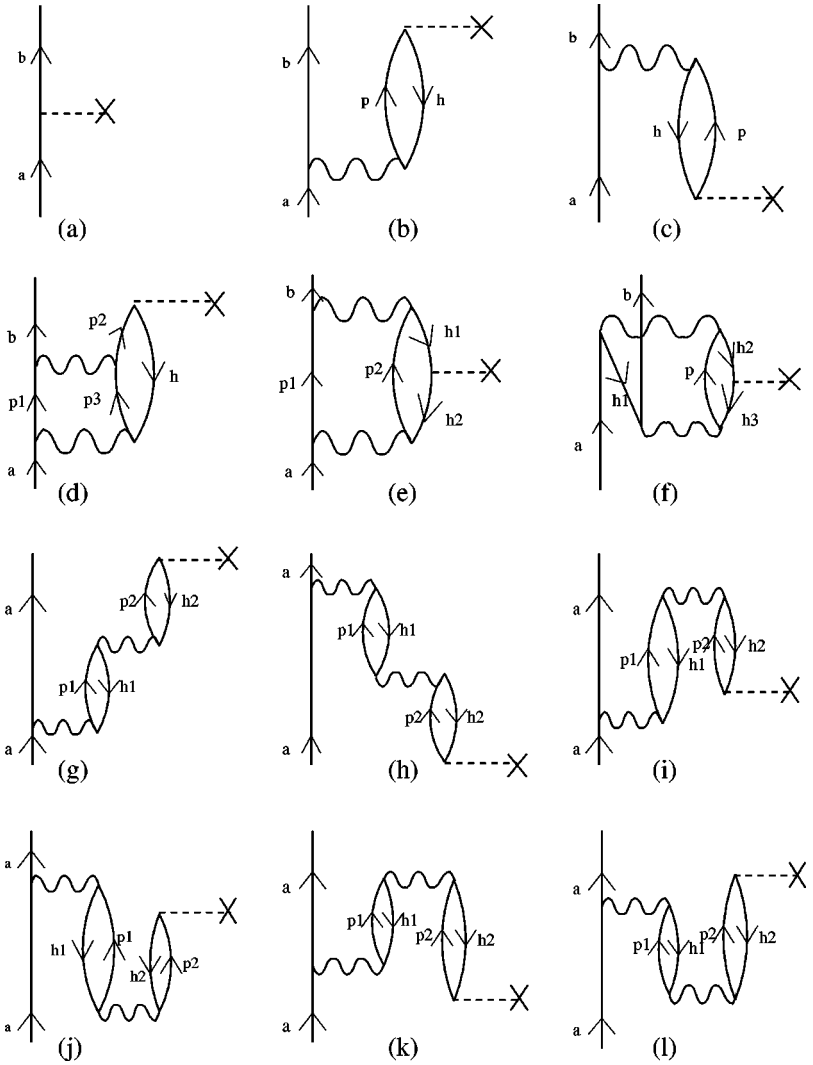

FIG. 2. (a) Zeroth- and (b), (c) first-order one-body diagrams for the effective charges. (d)–(f) illustrate some second order, (g) and (h) the TDA, and (i)–(l) the RPA diagrams included in the calculation of the effective charges.

the G-matrix with the wings mix center-of-mass and relative-coordinate configurations, as there is no orthogonal transformation between the two-particle states and the relative and center-of-mass coordinate states of the two interacting particles in this case. We checked the effect of mixing of the center-of-mass and relative-coordinate configurations in the $6\hbar\Omega$ calculation by varying the projection parameter used in the Hamiltonian and found that it is a very small effect.

In the no-core shell-model calculations presented here we calculate eigenenergies, electromagnetic properties using the bare nucleon charges, and the point-nucleon radii of ^{6}Li. In addition, we use the no-core shell-model calculation results for ^{5}He and ^{5}Li in Sec. V.

In order to gain insight into the model-space dependence of the no-core calculation, three different model spaces are investigated. For these three model spaces we use G-matrix elements evaluated in such a manner as to include all two-particle states with unperturbed energies up to $4\hbar\Omega$, $6\hbar\Omega$, and $8\hbar\Omega$ relative to the harmonic-oscillator ground state, corresponding to excitations of $2\hbar\Omega$, $4\hbar\Omega$, and $6\hbar\Omega$ above the lowest-energy configuration of ^{6}Li, respectively.

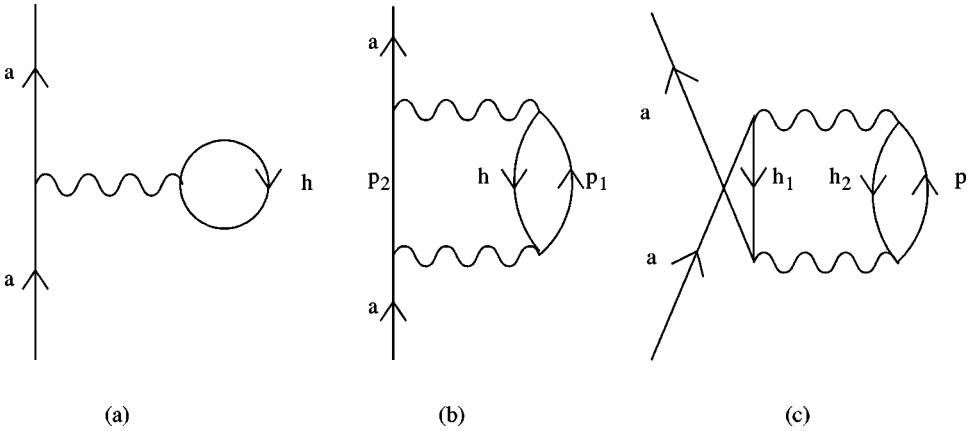

FIG. 3. First- and second-order one-body diagrams used to evaluate the single-particle energies.

B. Perturbation expansion

Once we have determined the G-matrix we may employ a perturbation expansion for effective operators calculated to second order to determine effective charges. The perturbation-expansion diagrams for effective operators included in our study follow the work of Siegel and Zamick [16]. Zeroth-order terms for effective charges are simply matrix elements of the bare operators. The two first-order terms, including their exchange diagrams, contain one intermediate state and have one interaction between the valence particles and the core particles. These zeroth-order and first-order diagrams are shown in Figs. 2(a)–2(c). The two first-order diagrams are evaluated as

$$\langle b|[O^{L\tau}a]^b\rangle=\sum_{p,h}(1+P_{ph})(-1)^{(L+\tau+j_p+j_h+1)}\frac{1}{\epsilon_b-(\epsilon_a+\epsilon_p-\epsilon_h)}\sum_{J,T}(2J+1)(2T+1)\sqrt{\frac{(2j_p+1)}{(2j_b+1)}}$$
$$\times\langle(j_bj_h)^{JT}|G|(j_aj_p)^{JT}\rangle W(L,j_p,j_b,J;j_h,j_a)W\left(\tau,\frac{1}{2},\frac{1}{2},T;\frac{1}{2},\frac{1}{2}\right)\langle p|[O^{L\tau}h]^p\rangle. \quad (5)$$

The operator P_{ph} exchanges the labels p and h, except for the energy denominator where its action results in the exchange of a and b. It changes diagram 2(b) into diagram 2(c). The quantities W are Racah coefficients and the reduced matrix element convention of Mavromatis, Zamick, and Brown [17] is employed, where the reduced matrix element $\langle p|[O^{L\tau}h]^p\rangle$ is defined by

$$\langle p|O^{L\tau}_M|h\rangle=(LMj_hm_h|j_pm_p)\langle p|[O^{L\tau}h]^p\rangle. \quad (6)$$

Instead of using approximate energy denominators set equal to multiples of $\hbar\Omega$, as done by Siegel and Zamick, we utilize energy denominators determined from calculated single-particle energies (e.g., ϵ_a) obtained using a second-order perturbation expansion that involves evaluating the three one-body diagrams, shown in Fig. 3. The formulas for these three diagrams are given in our study of effective interactions [18]. Using calculated single-particle energies will give a more accurate description of the differences in the energies of the particles involved in determining the energy denominators. All configurations up to $6\hbar\Omega$ above the ground state are included in the calculation of the energy denominators. The same single-particle energies were employed in all calculations, regardless of the size of the intermediate excitation space being used for the effective-operator diagrams.

Second-order terms for effective operators include all terms with two intermediate states and have two sets of interactions involving the core and excited particles. Some examples of the second-order diagrams for the effective charge are shown in Figs. 2(d)–2(l). Diagram (d) is an example of a second-order diagram obtained by inserting a G-interaction into a first-order diagram, in this case diagram (b). Figures 2(e) and 2(f) are examples of second-order diagrams, which have no counterpart in first-order. We do not include wave function renormalizations in the calculation.

In calculating the effective charges, the result for each diagram was divided by the zeroth-order diagram for normalization, thus the renormalized zeroth-order term is identically one for both the T=0 and T=1 cases, i.e., the isoscalar and isovector terms, respectively. The effective proton charge $e^{\rm p}_{\rm eff}$ and the effective neutron charge $e^{\rm n}_{\rm eff}$ are given in terms of the isoscalar effective charge $e^0_{\rm eff}$, evaluated with T=0, and the isovector effective charge $e^1_{\rm eff}$, evaluated with T=1, according to the following equations:

$$e^{\rm p}_{\rm eff}=\tfrac{1}{2}(e^0_{\rm eff}+e^1_{\rm eff}), \quad (7)$$

$$e^{\rm n}_{\rm eff}=\tfrac{1}{2}(e^0_{\rm eff}-e^1_{\rm eff}), \quad (8)$$

where $e^0_{\rm eff}$ and $e^1_{\rm eff}$ are determined by evaluating the different diagrams to various orders in the perturbation expansion (see Ref. [16], for example).

C. Model-space truncation

To make a direct comparison with the perturbation results we apply the model-space truncation formalism [5] to the no-core $6\hbar\Omega$ (or $4\hbar\Omega$) calculation in order to derive an equivalent description in the $0\hbar\Omega$ space. That is, we take the results of the large-space $6\hbar\Omega$ calculation and truncate (i.e., project) them into the $0\hbar\Omega$ space, so as to construct an effective $0\hbar\Omega$ Hamiltonian. The Lee-Suzuki starting-energy independent similarity transformation method [6] is used, which gives the effective Hamiltonian $PH_{\rm eff}P=PHP+PHQ\omega P$, with the transformation operator ω satisfying $\omega=Q\omega P$. This operator is obtained from the large-space $0\hbar\Omega$ dominated eigenstates using the relations

$$\langle\alpha_Q|k\rangle=\sum_{\alpha_P}\langle\alpha_Q|\omega|\alpha_P\rangle\langle\alpha_P|k\rangle, \quad (9)$$

$$\langle\alpha_Q|\omega|\alpha_P\rangle=\sum_{k\in\mathcal{K}}\langle\alpha_Q|k\rangle[\langle\alpha_P|k\rangle]^{-1}. \quad (10)$$

The states $|\alpha_Q\rangle$ and $|\alpha_P\rangle$ are the Q space and P space basis states, respectively, and $\mathcal{K}$ is the set of eigenstates $|k\rangle$ that we wish to reproduce in the truncated model space. Note that here the P space is the $0\hbar\Omega$ model space. Using this operator, the effective Hamiltonian can be constructed (see Ref. [7]), and a general effective operator is then obtained as [19–21]

TABLE I. No-core results for the ground-state energy (GE), electric quadrupole moment (E2), magnetic dipole moment (M1), and the root-mean-square point-proton radius (R_p) calculated in different model-space sizes for a G-matrix calculated with and without wings on the Q^P-operator.

	$2\hbar\Omega$		$4\hbar\Omega$		$6\hbar\Omega$		Experiment
Operator	wings	no wing	wings	no wing	wings	no wing	
GE [MeV]	−24.18	−26.82	−31.61	−32.23	−31.92	−32.07	−32.00
E2 [e fm^2]	−0.039	−0.108	−0.075	−0.109	−0.089	−0.092	−0.082
M1 [μ_N]	0.861	0.860	0.850	0.850	0.844	0.844	0.822
R_p [fm]	2.072	2.028	2.061	2.046	2.075	2.069	2.38

$$\overline{O}_{\text{eff}}=[P(1+\omega^{\dagger}\omega)P]^{-1/2}(P+P\omega^{\dagger}Q)\times\hat{O}(P+Q\omega P)[P(1+\omega^{\dagger}\omega)P]^{-1/2}. \quad (11)$$

In the particular application of this formalism to ^{6}Li, with $\hat{O}$ being one-body electromagnetic operators, we obtain, in general, two-body effective operators. These can be then separated into a one-body part with the help of effective charges and a two-body part [5].

III. NO-CORE CALCULATION RESULTS

The results using the large-model-space no-core calculations, with the G-matrix derived from the Nijmegen II potential, show good agreement with ^{6}Li experimental values, as shown in Table I. With the harmonic-oscillator parameter $\hbar\Omega = 14$ MeV, and the Δ of Eq. (2) chosen as -25 MeV to reproduce the experimental binding energy of ^{6}Li, the electric quadrupole moment, magnetic dipole moment, and root-mean-square proton radius, calculated in the $6\hbar\Omega$ model space, are all within about 10% of their respective experimental values.

From Table I we can see a very small dependence of the magnetic dipole moment of the ground state of ^{6}Li on the model-space size. Each successive increase in the size of the model space results in a smaller increase in the calculated value for the magnetic dipole moment. The calculated value of the magnetic dipole moment gets closer to the experimental value as the size of the model space increases.

The calculated root-mean-square proton radius is somewhat smaller than the experimentally determined value. There is a slight model-space dependence for the calculated value, where the calculated root-mean-square proton radius tends to increase as the size of the model space increases. This model-space dependence is too small to account for the discrepancy between the calculated and the experimentally determined values, the calculated value being about 15% smaller than the experimental value. This is a long-standing problem, where calculations which reproduce the correct binding energy tend to give a radius that is too small and calculations, which produce the correct radius, tend to underbind the system [22]. Since we have chosen to reproduce the correct binding energy by our choice of $\Delta = -25$ MeV in the starting energy, we can expect to calculate a radius that is too small.

No-core calculations of the electric quadrupole moment for the ground state of ^{6}Li closely match the small, negative experimental value of -0.082. Calculations performed in the $2\hbar\Omega$ model space give us a small, negative value that is on the order of the experimental value. Going to larger model spaces improves the result giving us a value that is very close to the experimental value for the electric quadrupole moment of ^{6}Li. The trend of convergence of the electric quadrupole moment with larger model spaces is not so consistent as the trend observed in the calculation of the magnetic dipole moment, discussed previously.

The difference between the results obtained in the no-core approach for the ground-state EM moments with and without wings depends upon the operator studied. For the magnetic dipole operator, the $0s_{1/2}$ state cannot be connected with the higher-lying states contained in the wings. Thus, there is no direct contribution to the magnetic dipole operator from the wing portion of the Q^P-operator and the effect of the wings upon the calculation of the magnetic dipole moment is essentially nonexistent. The root-mean-square proton radius exhibits a noticeable difference, when calculated with and without wings. In each of the model spaces studied the calculation with wings results in a smaller binding energy, increasing the radius. The wings also include states with a greater portion of their wave function at large radii. The combination of these two factors leads us to expect that calculations with wings will result in a greater calculated root-mean-square proton radius, which we observe in Table I. In all model spaces studied, including the wings in the calculation of the G-matrix causes the no-core calculated value of the electric quadrupole moment to be smaller than the calculation without the wings. The calculations for the electric quadrupole operator with and without wings grow closer together as we increase the size of the model space. The strong r^2-dependence and the contributions from the expanded portions of the model space cause the electric quadrupole moment to show the greatest dependence upon the wings of the three operators calculated. The number of states included in the wings decreases as we go to larger model spaces, so we would expect the difference between the calculations with and without wings to diminish in the larger model space calculations. The diminishing effect of the wings can be clearly seen in Table I.

IV. PERTURBATION CALCULATION RESULTS

We now turn to our study of the effective operators and effective charges obtained in the perturbation-expansion method. We utilize the same G-matrix as that used for the $6\hbar\Omega$ ^{6}Li no-core calculations discussed above. In evaluating the various diagrams, single-particle energies, calculated to second-order in perturbation expansion, were employed to

TABLE II. Results of perturbation-expansion calculations, showing the dependence of effective charges upon the type of energy denominators used. Results shown are for the $0p_{1/2}-0p_{3/2}$ transitions calculated without wave function renormalization diagrams. In the last two columns calculated single-particle energies (spe) are used (see Fig. 3).

2, 4, and $6\hbar\Omega$ excitation contributions to first- and second-order totals of $0p_{1/2}-0p_{3/2}$	multiples of $\hbar\Omega$		Calculated spe	
	T=0	T=1	T=0	T=1
$2\hbar\Omega$ excitations first-order	0.3270	−0.1493	0.2706	−0.1213
$2\hbar\Omega$ excitations second-order	−0.0992	−0.1289	−0.0288	−0.0712
$4\hbar\Omega$ excitations second-order	0.1171	−0.0244	0.0913	−0.0226
$6\hbar\Omega$ excitations second-order	0.0528	−0.0226	0.0530	−0.0218
Total 1st and 2nd order for all configurations within a given model space				
$2\hbar\Omega$ excitations 1st + 2nd total	0.2278	−0.2782	0.2418	−0.1925
$(2+4)\hbar\Omega$ excitations 1st + 2nd total	0.3449	−0.3026	0.3331	−0.2151
$(2+4+6)\hbar\Omega$ excitations 1st + 2nd total	0.3977	−0.3252	0.3861	−0.2369
0th + 1st + 2nd order	proton	neutron	proton	neutron
$(2+4+6)\hbar\Omega$ excitations	1.0363	0.3615	1.0746	0.3115

determine the energy denominators. These single-particle energies were calculated using

$$\epsilon_i = t_i + u_i , \tag{12}$$

where the u_i was determined by evaluating the first- and second-order diagrams shown earlier in Fig. 3. For the purpose of comparison with calculations done by others [16,23], all diagrams have also been evaluated using multiples of $\hbar\Omega$ for the energy denominators. The energy spacing between major shells using calculated single-particle energies, instead of multiples of $\hbar\Omega$, tends to be larger for the lower-lying states and smaller for the higher-lying states. The single-particle energies calculated using wings tended to be slightly larger than those calculated without wings, although this difference was less than 1%.

The difference in energy denominators using calculated single-particle energies results in about a 10% reduction in the $T=0$ and $T=1$ effective charges, when compared with the traditional method of using multiples of $\hbar\Omega$, as can be seen in Table II. Looking at the sum of the second-order diagrams in Table II, we see that the $2\hbar\Omega$ excitation space effective charges are much smaller, when using calculated energies, while there is less of a difference between the two methods for the effective charges calculated in the $4\hbar\Omega$ and $6\hbar\Omega$ intermediate-state excitation spaces. In the case of the 2 $\hbar\Omega$ excitation first- and second-order diagrams, the energy denominators obtained from calculated single-particle energies are larger and the resulting diagrams are smaller. All second-order diagrams have two energy denominators, which may have calculated energy gaps that are smaller than the energy gaps determined from multiples of $\hbar\Omega$, when we go to higher intermediate-state excitations. For example, a configuration included in the $6\hbar\Omega$ excitation space, but not in the $2\hbar\Omega$ or $4\hbar\Omega$ excitation spaces, may have one of the energy denominators corresponding to a $2\hbar\Omega$ excitation and one corresponding to a $6\hbar\Omega$ excitation. Thus the calculated energy denominator would be smaller than $6\hbar\Omega$ for the ''6 $\hbar\Omega$'' intermediate-state excitation and larger than $2\hbar\Omega$ for the ''$2\hbar\Omega$'' intermediate-state excitation. Hence, we will see less reduction, or even an enhancement, of the diagram using calculated single-particle energies, when compared to the same diagram evaluated using energy denominators that are $2\hbar\Omega$ and $6\hbar\Omega$. This effect can be clearly seen by looking at the $2\hbar\Omega$-excitation, $4\hbar\Omega$-excitation, and $6\hbar\Omega$-excitation contributions to the sum of the second-order diagrams, shown in Table II.

When effective-operator calculations in perturbation theory are compared, using a G-matrix computed with and without wings, there is less than a 1% difference for the electric quadrupole operator as well as the orbital and spin portion of the magnetic dipole operator. Similarly, the result of using single-particle energies calculated from G-matrix elements with and without wings also yields less than a 1% difference in the effective charges obtained from the effective operators. This result holds for the $2\hbar\Omega$, $4\hbar\Omega$, and $6\hbar\Omega$ model spaces as well as for first- and second-order calculations. Since we see only a small effect on effective-operator results from including the wings in the calculation of the G-matrix, we can safely conclude that the contribution of the wings plays no significant role in our perturbation-expansion calculations.

Because the calculations are done in a finite-sized model space, we also investigate the effect of including more intermediate states. For this portion of the study the same $8\hbar\Omega$ G-matrix elements, calculated using the Nijmegen II N-N potential, were used for all three choices for the intermediate-state excitations. The same energy denominators, determined from calculated single-particle energies, were also employed in all three calculations. The only difference between the three different intermediate-state calculations is that additional excited states have been included in the calculations. The largest intermediate-state space includes all the configurations that are included in the smaller spaces and obviously yields exactly the same results for these lower-lying configurations. Allowing a larger intermediate-state space will involve configurations at higher energies; these configurations will have larger energy denominators and the contribution from each higher-lying con-

TABLE III. Isoscalar and isovector components as well as proton and neutron quadrupole effective charges for various diagrams using calculated single-particle energies and an $8\hbar\Omega$ G-matrix with wings. Numbers listed are contributions due to the expanded portion of the intermediate-excitation space only, calculated without wave function renormalization diagrams.

	$0p_{1/2}-0p_{3/2}$				$0p_{3/2}-0p_{3/2}$			
	T = 0	T = 1	proton	neutron	T = 0	T = 1	proton	neutron
$2\hbar\Omega$ excitations 1st order	0.2706	−0.1213	0.0747	0.1960	0.2257	−0.1328	0.0464	0.1793
$4\hbar\Omega$ excitations 1st order								
$6\hbar\Omega$ excitations 1st order								
$2\hbar\Omega$ excitations 2nd order TDA	0.0517	0.0115	0.0316	0.0201	0.0478	0.0122	0.0300	0.0178
$4\hbar\Omega$ excitations 2nd order TDA	0.0158	0.0040	0.0099	0.0059	0.0146	0.0043	0.0095	0.0052
$6\hbar\Omega$ excitations 2nd order TDA	0.0036	0.0011	0.0023	0.0013	0.0033	0.0011	0.0022	0.0011
$2\hbar\Omega$ excitations 2nd order RPA								
$4\hbar\Omega$ excitations 2nd order RPA	0.0226	0.0048	0.0137	0.0089	0.0191	0.0053	0.0122	0.0069
$6\hbar\Omega$ excitations 2nd order RPA	0.0068	0.0017	0.0043	0.0025	0.0056	0.0020	0.0038	0.0018
$2\hbar\Omega$ excitations 2nd order total	−0.0289	−0.0712	−0.0500	0.0212	−0.0346	−0.0630	−0.0488	0.0142
$4\hbar\Omega$ excitations 2nd order total	0.0913	−0.0226	0.0344	0.0570	0.0854	−0.0212	0.0321	0.0533
$6\hbar\Omega$ excitations 2nd order total	0.0530	−0.0218	0.0156	0.0374	0.0506	−0.0211	0.0148	0.0358
$2\hbar\Omega$ excitations 1st + 2nd total	0.2418	−0.1924	0.0247	0.2171	0.1911	−0.1958	−0.0024	0.1935
$4\hbar\Omega$ excitations 1st + 2nd total	0.0913	−0.0226	0.0344	0.0570	0.0854	−0.0212	0.0321	0.0533
$6\hbar\Omega$ excitations 1st + 2nd total	0.0530	−0.0218	0.0156	0.0374	0.0506	−0.0211	0.0148	0.0358
0th + 1st + 2nd order total	1.3861	0.7632	1.0747	0.3115	1.3271	0.7619	1.0445	0.2826

figuration should be smaller. While the contribution of each individual configuration is generally smaller with a larger intermediate-excitation space, the number of configurations greatly increases with each increase in the excitation-space size.

The results of the effective-charge calculations for T=0 and T=1 in the various model spaces are shown in Table III. In the first-order diagrams, only the configurations that are exactly $2\hbar\Omega$ above the ground state contribute. This is because the operator involved is an interaction between the $0s_{1/2}$ hole state and a particle state, and only the $0d_{3/2}$ and $0d_{5/2}$ particle states have nonzero matrix elements of the transition operator with the $0s_{1/2}$ state. Having the hole states limited to the $0s_{1/2}$ state also excludes the possibility of a pure $2\hbar\Omega$ excitation configuration in the random phase approximation (RPA) diagrams shown in Figs. 2(e)–2(h).

Because there are no additional contributions to the zeroth- and first-order terms from excitations greater than $2\hbar\Omega$, we are left with only the second-order diagrams for investigating the intermediate-excitation space dependence. In general, the contribution from the expanded portion of the excitation space for each individual diagram decreases as the size of the intermediate space grows, although there are a few cases where the $6\hbar\Omega$ excitation contribution is of the same size or slightly larger than the $4\hbar\Omega$ excitation contribution, which is in turn of the same size or larger than the $2\hbar\Omega$ excitation contribution for the same diagram.

Siegel and Zamick [16] also study the effect of going to a larger excitation space. Their method of determining the excitation space differs from the one in this study, in that they restrict their space by allowing all configurations for particles within a given shell. In the current study we restrict the intermediate excitation-space to all configurations within a given energy limit. The calculations by Siegel and Zamick leave out configurations with a single-particle in a high-lying shell and a lower energy than some of their included configurations. The calculation in the current study does not include configurations obtained within a given shell that are at higher energies than the limit set on intermediate-state excitations. Some conclusions can still be drawn from the similarities of going to larger excitation spaces. Siegel and Zamick [16] looked at the convergence of the TDA and RPA diagrams and assumed that these diagrams would adequately estimate the effect of intermediate-space truncation. Their calculations show that the contributions from the larger excitation space for the TDA and RPA graphs are about one order of magnitude smaller than the contribution from the smaller excitation spaces. In our calculation the contribution from each of the successively larger excitation spaces decreases by roughly a factor of 4 for the TDA and RPA diagrams. Yet, when we calculate the sum of all second-order diagrams, we do not observe the same convergence that was found for the TDA and RPA studies. In fact, the second-order total contributions from the different intermediate-state spaces are of comparable magnitude and some are even of different sign. This can be seen both in the results for T=0 and T=1, and in the effective proton and neutron charges, as shown in Table III. The intermediate-state excitation-space truncation does not show strong convergence, although the major contribution to the effective charges does come from $2\hbar\Omega$ excitation contributions.

In studying the order-by-order convergence of the diagrams, we see again that the diagrams evaluated with T=0 show better convergence than the diagrams evaluated with T=1. This is just the opposite of the result found for the convergence of the effective interaction in Ref. [24]. The second-order diagrams are all significantly smaller than the two first-order diagrams for T=0. The sum of second-order

TABLE IV. Second order terms in the perturbation-expansion calculation of the magnetic dipole moment of ^{6}Li using calculated single-particle energies and an $8\hbar\Omega$ G-matrix with wings. $N\hbar\Omega$ means the sum of all contributions from 2 to $N\hbar\Omega$.

Excitation	$0p_{1/2}-0p_{1/2}$		$0p_{1/2}-0p_{3/2}$		$0p_{3/2}-0p_{3/2}$	
Space	T = 0	T = 1	T = 0	T = 1	T = 0	T = 1
$2\hbar\Omega$ l-part	−0.0765	0.0243	−0.0135	0.0147	0.0279	0.0213
$4\hbar\Omega$ l-part	−0.1020	0.0410	−0.0220	0.0253	0.0307	0.0361
$6\hbar\Omega$ l-part	−0.1146	0.0527	−0.0296	0.0310	0.0267	0.0432
$2\hbar\Omega$ s-part	0.0174	−0.0439	−0.0135	−0.0364	0.0375	−0.0228
$4\hbar\Omega$ s-part	0.0329	−0.0537	−0.0220	−0.0452	0.0753	−0.0286
$6\hbar\Omega$ s-part	0.0400	−0.0560	−0.0319	−0.0481	0.0943	−0.0304
	$0p_{1/2}-0p_{1/2}$		$0p_{1/2}-0p_{3/2}$		$0p_{3/2}-0p_{3/2}$	
	proton	neutron	proton	neutron	proton	neutron
$6\hbar\Omega$ l-part	−0.0310	−0.0837	0.0007	−0.0303	0.0350	−0.0083
$6\hbar\Omega$ s-part	−0.0080	0.0480	−0.0400	0.0081	0.0320	0.0623

diagrams is about an order-of-magnitude smaller than the sum of the two first-order diagrams. The second-order diagrams for T=1 are all individually smaller than the two first-order diagrams, but the sum of the second-order T=1 diagrams is approximately the same size as the sum of the two first-order T=1 diagrams.

When the isoscalar and isovector contributions are combined to produce proton and neutron effective charges, via Eqs. (7) and (8), the different convergence trends for the T=0 and T=1 diagrams cause problems for the convergence of the effective proton and neutron charges. The neutron effective charge is dominated by the $2\hbar\Omega$ first-order diagrams, being about twice the size of the sum of all second-order diagrams. The proton effective charge does not show a similar dominating term. The second-order totals show a strong excitation space dependence. The $4\hbar\Omega$ and $6\hbar\Omega$ second-order totals are of opposite sign and similar magnitude to the $2\hbar\Omega$ second-order total and tend to cancel any major contribution from the second-order diagrams. It is unclear if going to larger excitation spaces will result in any significant contributions from second-order diagrams. Although the RPA and TDA diagrams show good convergence as the excitation space increases, other second-order diagrams, particularly ones of opposite sign, counteract this convergence trend. The sum of all second-order diagrams is marginally largest for the $2\hbar\Omega$ excitation contributions for the effective proton charge but the same cannot be said for the effective neutron charge.

The effective neutron charge is of the order of 0.3 with about two-thirds of this coming from the first-order diagram. The effective proton charge is slightly larger than 1, with the major contribution coming from first-order and, at least in a $6\hbar\Omega$ excitation space, no significant contribution coming from second-order diagrams.

The results for the perturbation-expansion calculation of the magnetic-dipole moments of ^{6}Li are shown in Table IV. As the size of the excitation space increases, the convergence of the T=0 and T=1 elements is well behaved for both the orbital and spin portion of the dipole moment matrix elements. The best convergence occurs in the T=1 spin contribution to the magnetic-dipole operators, where each increase of $2\hbar\Omega$ in the excitation space gives an additional contribution, which is approximately one fourth of the lower-excitation-space contribution. In these particular matrix elements the major contribution comes from the $2\hbar\Omega$ excitation configurations with relatively small contributions from higher-lying excitations, which tend to decrease as the excitation energy gets larger.

The vast majority of the diagrams used to evaluate the magnetic-dipole operator give zero contribution due to the relatively small number of nonzero bare magnetic-dipole matrix elements. The bare M1 matrix element is nonzero only when the initial and final states of the operator have the same quantum numbers n, l. Thus, all first-order diagrams, shown in Fig. 2, give zero contribution to the magnetic-dipole operator because the operator cannot connect a $0s_{1/2}$ hole state with a higher lying particle state. Since the zeroth-order contribution does not change and the first-order contribution is identically zero for all states, it is difficult to make any statement about the order-by-order convergence of the perturbation expansion. Even the TDA and RPA diagrams, which have traditionally been evaluated to higher order in calculations of other effective operators, are identically zero, so we are unable to pursue the order-by-order convergence of the magnetic-dipole operator any further.

The results obtained from perturbation-theory calculations of the magnetic-dipole operator are consistent with results obtained from other calculations [17,25]. All of the TDA and RPA diagrams, which we evaluate to give zero contribution, also have zero contribution in other studies involving one or two nucleons outside a doubly magic closed shell. The second-order corrections to the magnetic-dipole operator are small with the majority contribution to these operators coming from the zeroth-order term.

V. MODEL-SPACE TRUNCATION RESULTS: A AND $\hbar\Omega$ DEPENDENCE

For a direct comparison with the effective charges obtained in the perturbation-expansion calculation, we calculate the effective charges in the model-space truncation scheme, as described in Ref. [5], employing the same interaction used

TABLE V. Effective charges of the proton and neutron quadrupole, magnetic orbital, and magnetic spin operators, derived by least-square fits to the corresponding $0p$-shell effective operators obtained by model-space truncation method from the $6\hbar\Omega$ calculation for ^{6}Li using the ''single-valued'' G-matrix with wings, $\Delta=-25$ MeV, and $\hbar\Omega=14$ MeV. Both the j-dependent and j-independent effective charges are shown. Also, the j-independent effective charges obtained in the same way from the $4\hbar\Omega$ calculation are presented in the last two columns, labeled eff-4.

	$e^{\rm p}_{1/23/2}$	$e^{\rm n}_{1/23/2}$	$e^{\rm p}_{3/23/2}$	$e^{\rm n}_{3/23/2}$	$e^{\rm p}_{1/21/2}$	$e^{\rm n}_{1/21/2}$
E2	1.184	0.272	1.080	0.215		
Ml	0.890	0.036	0.954	0.061	0.910	0.068
Ms	0.939	−0.012	0.972	−0.001	0.943	−0.031
	$e^{\rm p}_{\rm eff}$	$e^{\rm n}_{\rm eff}$	$e^{\rm p}_{\rm eff\text{-}4}$	$e^{\rm n}_{\rm eff\text{-}4}$		
E2	1.141	0.245	1.087	0.189		
Ml	0.934	0.061	0.948	0.047		
Ms	0.955	−0.005	0.966	−0.005		

in the perturbation calculation, namely, a ''single-valued'' G-matrix (as opposed to the effective interaction used later in this section) with wings, obtained with the Nijmegen II N-N potential, a harmonic-oscillator parameter $\hbar\Omega=14$ MeV, and a fixed $\Delta=-25$ MeV. The effective charges computed with this interaction are shown in Table V and compared with the corresponding perturbation results in Table VI. These comparisons are for the one-body part of the one-plus-two-body effective operators obtained in this approach (see Ref. [5]). The real two-body part is found to be small, typically not more than 10% of the full operator.

Our previous calculations of effective charges, published in Ref. [5], employed a different effective two-nucleon interaction, the so-called ''multivalued'' interaction introduced in Ref. [11]. In this method, different Q^P-operators are utilized in evaluating the G-matrix for configurations with different spectator energies, hence the name ''multivalued'' G-matrix approach. The effective interaction employed in Ref. [5] also uses the Reid93 N-N potential [10] and a harmonic-oscillator parameter of $\hbar\Omega=17.2$ MeV.

A comparison of the effective charges from Table III of Ref. [5] and Table V in the present paper shows that the quadrupole effective charges obtained here with the ''single-valued'' G-matrix are considerably smaller than those obtained with the ''multivalued'' G-matrix. A major factor in this difference is the choice of the harmonic-oscillator parameter. To understand the dependence of the quadrupole effective charges on $\hbar\Omega$, we performed separate calculations, as described later. The $\hbar\Omega$ dependence accounts for some of the difference between the two sets of effective charges, but the interactions used in the calculations also contribute to this difference. The electromagnetic transitions are weaker in the ''single-valued'' calculation, which implies smaller contributions to the effective charges. As to the comparison with the experiment, the ''multivalued'' interaction gives superior results. Therefore, the effective charges extracted from the ''multivalued'' interaction calculation should also be more realistic.

To gain a deeper insight into the dependence of the quadrupole effective charge on $\hbar\Omega$ and A, we performed several additional calculations. In Fig. 4 we present the quadrupole effective proton, neutron (a), isoscalar (b), and isovector (c) effective charge dependence on $\hbar\Omega$ and A. The effective charges were obtained by the model-space truncation method, going from the $6\hbar\Omega$ relative to the unperturbed ground state to the $0\hbar\Omega$ model space in calculations for ^{6}Li and ^{5}He,^{5}Li. The $A=5$ results were extracted from the calculations presented in Fig. 1 of Ref. [7]. The calculations were performed for a wide range of the harmonic-oscillator frequencies, $\hbar\Omega$=8, 10, 14, 17.8, and 22 MeV. The $A=6$ results obtained for $\hbar\Omega=17.2$ MeV are taken from Ref. [5]. Two more $A=6$ calculations, for $\hbar\Omega=14$ and 20 MeV, were performed, using the same approach. All the calculations use the ''multivalued'' isospin-invariant effective interaction derived from the Reid93 potential, as described in Ref. [7]. The effective charges are trivially computed for the

TABLE VI. Comparison of effective charges obtained through a perturbation-expansion calculation and a model-space-truncation calculation. Both results are for a ''single-valued,'' $8\hbar\Omega$ G-matrix with wings derived using the Nijmegen II N-N potential, $\Delta=-25$ MeV, and $\hbar\Omega=14$ MeV.

	$0p_{1/2}-0p_{1/2}$		$0p_{1/2}-0p_{3/2}$		$0p_{3/2}-0p_{3/2}$	
	proton	neutron	proton	neutron	proton	neutron
E2 perturbation			1.07	0.31	1.04	0.28
E2 space truncation			1.18	0.27	1.08	0.22
M1l perturbation	0.97	−0.08	1.00	−0.03	1.04	−0.01
M1l space truncation	0.91	0.07	0.89	0.04	0.95	0.06
M1s perturbation	0.99	0.05	0.96	0.01	1.03	0.06
M1s space truncation	0.94	−0.03	0.94	−0.01	0.97	−0.001

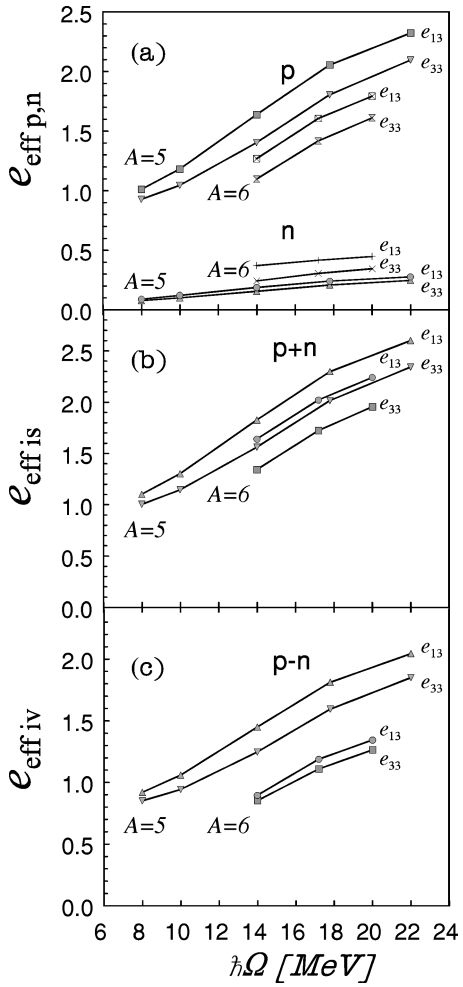

FIG. 4. (a) The quadrupole effective proton, neutron, (b) isoscalar, and (c) isovector effective charge dependence on $\hbar\Omega$ and A. The effective charges were obtained by the model-space truncation from $6\hbar\Omega$ calculations for ^{6}Li and ^{5}He,^{5}Li. The $A=5$ results correspond to the calculation presented in Fig. 1 of Ref. [7], obtained for $\hbar\Omega=8$, 10, 14, 17.8, and 22 MeV. The $A=6$ results, obtained for $\hbar\Omega=17.2$ MeV, are taken from Ref. [5]. Two additional calculations, for $\hbar\Omega=14$ and 20 MeV, are presented. All the calculations use the ''multivalued'' effective interaction derived from the Reid93 potential, as described in Ref. [7].

$A=5$ system by taking the ratios of the matrix elements calculated in the $6\hbar\Omega$ space with the corresponding ones from the $0\hbar\Omega$ space, e.g.,

$$e^{\mathrm{p}}_{\mathrm{eff}33}=\langle \tfrac{3}{2}^-(6\hbar\Omega,{}^5\mathrm{Li})\big|Q^{(2)}\big|\tfrac{3}{2}^-(6\hbar\Omega,{}^5\mathrm{Li})\rangle\Big/ \langle \tfrac{3}{2}^-(0\hbar\Omega,{}^5\mathrm{Li})\big|Q^{(2)}\big|\tfrac{3}{2}^-(0\hbar\Omega,{}^5\mathrm{Li})\rangle.$$

The one-body quadrupole operator used in the calculations employs free nucleon charges. The $A=6$ effective charges are obtained using the method described in Ref. [5].

From Fig. 4 we observe an almost linear scaling of the effective charges. This can be simply understood. In particular, for the $A=5$ results, it is apparent that such scaling exists under the condition that the large-space, here $6\hbar\Omega$, results depend only weakly on $\hbar\Omega$. The $0\hbar\Omega$ results, on the other hand, are proportional to the harmonic-oscillator parameter $b^2=(\hbar c)^2/(m_{\mathrm{N}}c^2\hbar\Omega)$. Therefore, $e_{\mathrm{eff}}(\hbar\Omega_1)\approx(\hbar\Omega_1/\hbar\Omega_2)e_{\mathrm{eff}}(\hbar\Omega_2)$. Apparently, and not surprisingly, the scaling persists for $A=6$ as well.

A more nontrivial result is, however, the observation that the isoscalar effective charges remain almost the same for $A=5$ and $A=6$, while, on the other hand, there is a significant change in the isovector effective charges. This can be seen by comparing parts (b) and (c) of Fig. 4. In fact, a similar A dependence was reported by Nakada and Otsuka in Ref. [26] in a phenomenological shell-model calculation for the p-shell nuclei. Here we make a similar observation in a microscopic calculation.

Let us return to the comparison of the effective charges obtained from the ''single-valued'' effective interaction, Table V, and from the ''multivalued'' interaction, Table III, of Ref. [5]. From the above discussion of the $\hbar\Omega$ dependence, we should expect the electric-quadrupole effective charges, calculated with $\hbar\Omega=17.2$ MeV, to be larger by a factor of $17.2/14\approx1.23$. The remaining difference in the effective charges should then be attributed to the differences in the two effective interactions.

VI. CONCLUSIONS

To summarize, the goal of this project was to study different microscopical approaches for calculating the electromagnetic operators of light nuclei, and in particular, ^{6}Li. As in Ref. [18] for the effective interaction, the no-core calculation was again used as a ''theoretical experiment'' and as a starting point for the model-space truncation calculation for the purpose of comparison with the standard perturbation-theory calculations of effective operators. The results for the electric quadrupole operator give us more information about perturbation-theory calculations of effective operators than the results of the magnetic dipole calculation. For the electric quadrupole operator we find that the use of single-particle energies, instead of multiples of $\hbar\Omega$, for the energy denominators has a small effect, favoring larger effective proton and neutron charges for calculations with energy denominators, which are multiples of $\hbar\Omega$. Hence, in perturbation-theory calculations of effective charges, calculated single-particle energies appear to have no advantage over multiples of $\hbar\Omega$.

Similar to previous perturbation-theory calculations of effective charges [3,16,23], we find that the perturbation expansion does not converge rapidly. In addition, we discover, as seen in Tables III and IV, that the second-order terms are not well-behaved as the size of the space increases. This is opposite to the conclusion of Siegel and Zamick [16], based only on the RPA and TDA terms (which are also well-behaved with space size in our calculations). It is unclear whether going to larger excitation spaces and/or higher-orders in the perturbation expansion will change the conclusions based on the present results.

Unlike the calculation for the effective interaction, the order-by-order convergence of the perturbation expansion for effective charges is better for $T=0$ states than for $T=1$ states [18,24]. When we look at the proton and neutron effective charges computed in the perturbation theory, we see that the proton effective charge has small and opposite contributions coming from the first- and second-order terms, while the effective neutron charge has its first-order contri-

bution about twice as large and of the same sign as the second-order contribution. The effective charges that we obtain, $e_n \approx 0.3$ and $e_p \approx 1.1$, are similar to the effective charges obtained in other perturbation calculations for larger nuclei. The effective charges obtained through a perturbation expansion show good agreement with the effective charges obtained through a model-space truncation calculation, when the same interaction and harmonic-oscillator parameter are used.

Since the zeroth-order effective charges are fixed and the first-order contributions are zero for the magnetic dipole operator, there is little that can be concluded about the convergence of this operator. It is worth noting that there is very little contribution to both the orbital and the spin portion of the magnetic-dipole operator from second-order. This is consistent with the findings of the model-space-truncation results for effective magnetic-dipole charges, i.e., g-factors. Similar to the findings from the calculation of the electric-quadrupole operator, the effective charges we obtain from the perturbation expansion for the magnetic dipole operator are of the same size as effective charges obtained in the model-space-truncation calculation, when using the same ''single-valued'' G-matrix in both calculations, as summarized in Table VI.

We have also studied the $\hbar\Omega$ and the A dependence of the E2 effective charges in the model-space-truncation method. We used the $6\hbar\Omega$ calculations for ^{5}Li, ^{5}He, and ^{6}Li, performed for a wide range of the harmonic-oscillator frequencies and using the ''multivalued'' effective interaction derived from the Reid93 potential, to extract the $0\hbar\Omega$ effective charges. We find a scaling of the effective charges with $\hbar\Omega$, which can be simply understood. Let us mention that the effective charges extracted from the experimental E2 transitions or moments depend on the value of $\hbar\Omega$ used in the analysis and would scale with $\hbar\Omega$ in a similar manner as we observe in our microscopic calculations. Typically, the appropriate values of $\hbar\Omega$ employed in such analyses were taken from a standard formula, such as $\hbar\Omega = 45A^{-1/3} - 25A^{-2/3}$ MeV. For $A=6$ this gives 17.2 MeV, the same value we utilized in our calculations in Ref. [5], and for which we obtained effective charges consistent with the experimental ones. Also, we observe different behavior of the isoscalar and isovector effective charges with respect to a change in the mass number A. While the isoscalar charges remain almost constant as a function of A, the isovector charges change significantly between $A=5$ and $A=6$. A similar observation for other p-shell nuclei was reported in Ref. [26]. There is also a dependence of the effective charge on the strength of the effective interaction used in the calculation. We obtain the significant result that the ''multivalued'' effective interaction yields more realistic values for the effective charges than the ''single-valued'' effective interaction.

ACKNOWLEDGMENTS

This material is based upon work supported by the National Science Foundation under Grant No. PHY96-05192. P.N. also acknowledges partial support from the grant of the Grant Agency of the Czech Republic 202/96/1562.

[1] C. Bloch and J. Horowitz, Nucl. Phys. **8**, 91 (1958); B. H. Brandow, Rev. Mod. Phys. **39**, 771 (1967).
[2] M. Hjorth-Jensen, T. T. S. Kuo, and E. Osnes, Phys. Rep. **261**, 125 (1995), and references therein.
[3] P. J. Ellis and E. Osnes, Rev. Mod. Phys. **49**, 777 (1977), and references therein.
[4] N. LoIudice, D. J. Rowe, and S. S. M. Wong, Phys. Lett. **37B**, 44 (1971); Nucl. Phys. **A219**, 171 (1974); P. Federman and S. Pittel, Phys. Lett. **77B**, 128 (1978).
[5] P. Navrátil, M. Thoresen, and B. R. Barrett, Phys. Rev. C **55**, R573 (1997).
[6] K. Suzuki and S. Y. Lee, Prog. Theor. Phys. **64**, 2091 (1980).
[7] P. Navrátil and B. R. Barrett, Phys. Rev. C **54**, 2986 (1996).
[8] B. R. Barrett, R. G. L. Hewitt, and R. J. McCarthy, Phys. Rev. C **3**, 1137 (1971).
[9] H. A. Bethe, B. H. Brandow, and A. G. Petschek, Phys. Rev. **129**, 225 (1963).
[10] V. G. J. Stoks, R. A. M. Klomp, C. P. F. Terheggen, and J. J. de Swart, Phys. Rev. C **49**, 2950 (1994).
[11] D. C. Zheng, B. R. Barrett, J. P. Vary, W. C. Haxton, and C. L. Song, Phys. Rev. C **52**, 2488 (1995).
[12] T. H. Schucan and H. A. Weidenmüller, Ann. Phys. (N.Y.) **73**, 108 (1972); **76**, 483 (1973).
[13] A. G. M. van Hees and P. W. M. Glaudemans, Nucl. Phys. **A396**, 105 (1983).
[14] P. J. Brussaard and P. W. M. Glaudemans, *Shell-Model Applications in Nuclear Spectroscopy* (North-Holland, Amsterdam, 1977).
[15] E. Baranger and C. W. Lee, Nucl. Phys. **22**, 157 (1961).
[16] S. Siegel and L. Zamick, Nucl. Phys. **A145**, 89 (1970).
[17] H. A. Mavromatis, L. Zamick, and G. E. Brown, Nucl. Phys. **80**, 558 (1966).
[18] M. Thoresen, D. C. Zheng, and B. R. Barrett, Phys. Rev. C **53**, 1997 (1996).
[19] P. Navrátil, H. B. Geyer, and T. T. S. Kuo, Phys. Lett. B **315**, 1 (1993).
[20] T. T. S. Kuo, P. J. Ellis, Jifa Hao, Zibang Li, K. Suzuki, and R. Okamoto, Nucl. Phys. **A560**, 621 (1993).
[21] K. Suzuki and R. Okamoto, Prog. Theor. Phys. **93**, 905 (1995).
[22] J. W. Negele, Rev. Mod. Phys. **54**, 913 (1982).
[23] P. J. Ellis and S. Siegel, Phys. Lett. **34B**, 177 (1971).
[24] M. Hjorth-Jensen, H. Müther, E. Osnes, and A. Ploos, J. Phys. G **22**, 321 (1996).
[25] A. E. L. Dieperink and P. J. Brussaard, Nucl. Phys. **A129**, 33 (1969).
[26] H. Nakada and T. Otsuka, Phys. Rev. C **49**, 886 (1994).